

Materials Science

An Indian Journal

Full Paper

MSAIJ, 12(9), 2015 [326-333]

Study of some characteristics describing the oxidation of a {m, m'}-based {30Cr, 1C, 15Ta} containing alloy during heating up to high temperature and the oxide scales behavior during post-{isothermal stage} cooling. part 3: {m, m'}={Fe, Ni}

Gaël Pierson^{1,2}, Kevin Duretz^{1,2}, Thierry Schweitzer², Elodie Conrath³, Patrice Berthod^{1,2,3*}

¹University of Lorraine, (FRANCE)

²Faculty of Sciences and Technologies, (FRANCE)

³Institut Jean Lamour (UMR 7198), Team 206 "Surface and Interface, Chemical Reactivity of Materials"

B.P. 70239, 54506 Vandoeuvre-lès-Nancy, (FRANCE)

E-mail : Patrice.Berthod@univ-lorraine.fr

ABSTRACT

An alloy based on iron and nickel in equal parts, rich in chromium and containing a dense TaC network in its microstructure was tested in oxidation at high temperature in dry synthetic air. The thermogravimetry tests were performed at 1000, 1100 and 1200°C during 40 hours. The mass gain files were plotted versus temperature and exploited to specify the oxidation start during heating and spallation start during cooling temperatures as well as the successive parts of mass gain achieved during heating and during the isothermal stage. The mass gain kinetic at 1000°C is quite parabolic and the rate rather low. The mass gain curves obtained at 1100 and 1200°C are in contrast affected by the occurrence of mass gain jumps. The oxidation kinetic during the heating and the isothermal stage are closer to the one of the NiCo-based alloy previously studied than to the CoFe-based one. Concerning the behaviour of the oxide scale during the post-isothermal stage cooling the behaviour of this FeNi-based alloys is similar to the two others alloys' one, as is to say severe spallation also occurred here. Metallographic characterization will be soon undertaken for the three alloys.

© 2015 Trade Science Inc. - INDIA

KEYWORDS

Iron;
Nickel;
Tantalum carbides;
High temperature oxidation;
Oxide spallation.

INTRODUCTION

Iron and nickel are often combined together into alloys able to work at high temperature as well as in cryogenic conditions. At all temperatures their austenitic matrix brings high mechanical strength and preserves a minimal ductility. Even if mechanical resistance and

high hardness may be achieved by other means as fast solidification^[1] or heat-treatment/quenching^[2] for bulk^[3] or coating^[4] iron-based alloys and by chromium carbides^[10-12] for nickel-based alloys, other reinforcing particles may be considered. This is the case of the tantalum carbides which display both intrinsic high hardness and mechanical resistance, but also which crystal-

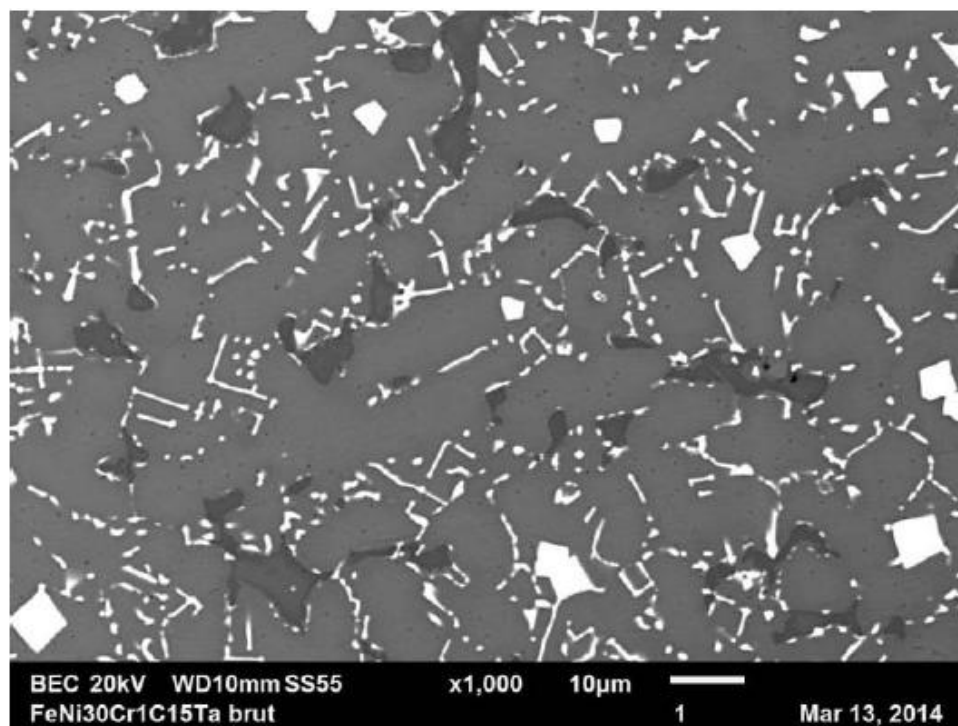


Figure 1 : SEM/BSE micrograph illustrating the as-cast microstructure of the studied alloy

lize at solidification as script-like carbides forming an eutectic with the matrix. Furthermore, for the applications at elevated temperatures, their good stability allows a persistence of their strengthening effect on long times.

Associating a chromium-rich Fe-Ni austenitic matrix with high TaC fraction was explored in a previous work^[9] in which, after preliminary thermodynamic calculations, a 30wt.%Cr-containing {Fe, Ni}-based alloy with 1wt.%C and 15wt.%Ta was elaborated and its as-cast microstructure studied. The purpose of this work is now to explore the behaviour of this alloy in hot oxidation, by exposing it to air at temperature ranging from 1000 and 1200°C.

EXPERIMENTAL

The chemical composition of the studied alloy was initially targeted to be 30wt.%Cr, 1wt.%C, 15wt.%Ta, and equal contents in iron and nickel: 27wt.% each of them. As previously specified by Energy Dispersive Spectrometry^[9], the obtained composition was 28.43±0.76wt.%Fe, 27.06±0.91wt.%Ni, 31.60±0.43wt.%Cr, and 12.91±1.92wt.%Ta (the carbon content being not controllable by EDS). The as-

cast microstructure of the alloy is illustrated in Figure 1 by a micrograph taken with a Scanning Electron Microscope (SEM) in Back Scattered Electrons (BSE) mode. The white particles are TaC carbides, the blocky ones of a probably pre-eutectic origin and the script-like ones of an obvious eutectic one. Some chromium carbides are also present (the dark particles). The matrix is composed of two parts: the palest one is probably an austenitic iron-nickel solid solution containing chromium, and a ferritic darker one containing chromium in especially high content. Their surface fractions, as measured by image analysis, were 4.19±0.90 surf.% for the ferritic part of matrix and 8.77±1.77 surf.% for the tantalum carbides.

During the cutting performed to obtain the part for the metallographic examinations, three parallelepipeds of about 3mm × 7mm × 7 mm were also prepared. These ones were ground with SiC papers of grade 1200 on their six faces, with which their edges and corners were also smoothed. The oxidation tests were run using a SETARAM TGA92 92-16.18 thermo-balance, under a flow of dry synthetic air (80%N₂-20%O₂). The heating was realized at +20K min⁻¹, the isothermal stage at 1000, 1100 or 1200°C for 40 hours, and the cooling rate at -5K min⁻¹.

Full Paper

The mass variations were recorded every 32 (test at 1000°C) or 33 (1100 & 1200°C) seconds. The mass gain files were corrected from the air buoyancy variations and plotted as mass gain versus temperature and exploited to specify the following characteristics:

Heating

- temperature at which the mass gain is significant enough to be detected by the micro-balance,
- eventual determination of the activation energy (if linear part in the curve describing the instantaneous linear mass gain rate variation with temperature, plotted according to the Arrhenius scheme),
- total mass gain achieved during the whole heating between the start of oxidation and the beginning of the isothermal stage),
- final linear mass gain rate when temperature reaches the isothermal stage one;

Isothermal stage

- global shape of the mass gain curve when plotted versus time (parabolic or not, jumps or not),
- total mass gain exclusively achieved during the isothermal stage;

Cooling

- Temperature at which the mass variation accelerates or becomes irregular (start of scale spallation),
- Final mass variation.

RESULTS AND DISCUSSION

Oxidation during heating

The heating parts of the mass gain curves plotted versus temperature are presented together in Figure 2. It appears first that the common parts of the 1000°C-curve and the 1200°C curve (up to 1000°C) are superposed while the 1100°C-curve's one seems slightly shifted. The temperatures of oxidation start (defined as being the ones at which the mass gain is high enough to be detected by the thermo-balance) are rather close to one another (TABLE 1), over a 20°C-wide range only.

Over these temperatures of oxidation start the in-

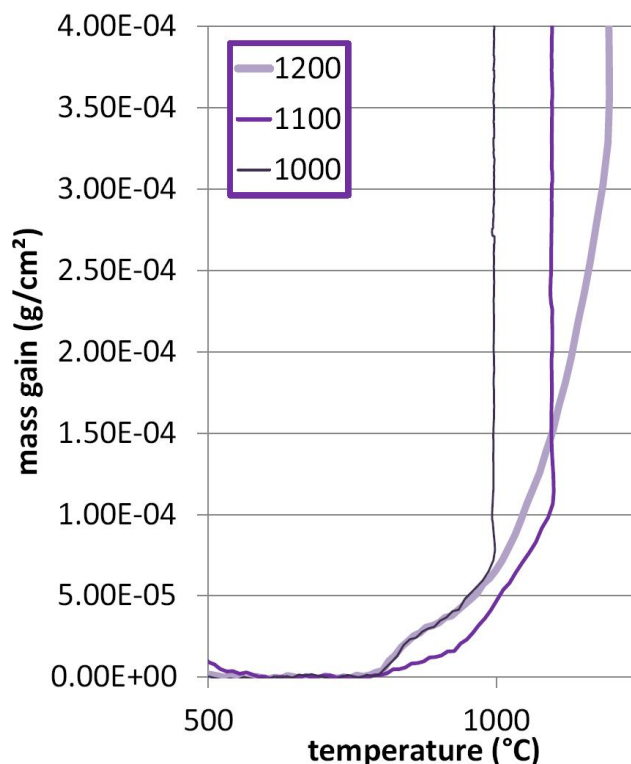


Figure 2 : Enlarged view of the mass gain curves recorded during heating until reaching 1000, 1100 or 1200°C

TABLE 1 : Values of the temperatures at which the mass gain by oxidation during heating has become significantly high enough

1000°C-test	1100°C-test	1200°C-test	reproducibility
785.9	799.6	780.7	rather good

stantaneous linear kinetic constant increases more and more rapidly when temperature increases during the heating, this letting thinking here too to an exponential increase with temperature. The Arrhenius plot confirms this over the whole heating from oxidation start or only on the high temperature part of the heating, since the points' clouds are globally elongated along a straight line. The slope of the regression straight line led to the values of activation energies listed in the first line of TABLE 2. They are rather scattered since their values are in the 42-120kJ/Mol range. The second line of TABLE 2 contains the values of the final value of $(d\Delta m/S)/dt$ when temperature reaches the stage one. This ultimate value of K_1 effectively increases with temperature, showing that oxidation is, at the beginning of the isothermal stage, logically faster when the stabilized temperature is higher. The mass gains achieved during the

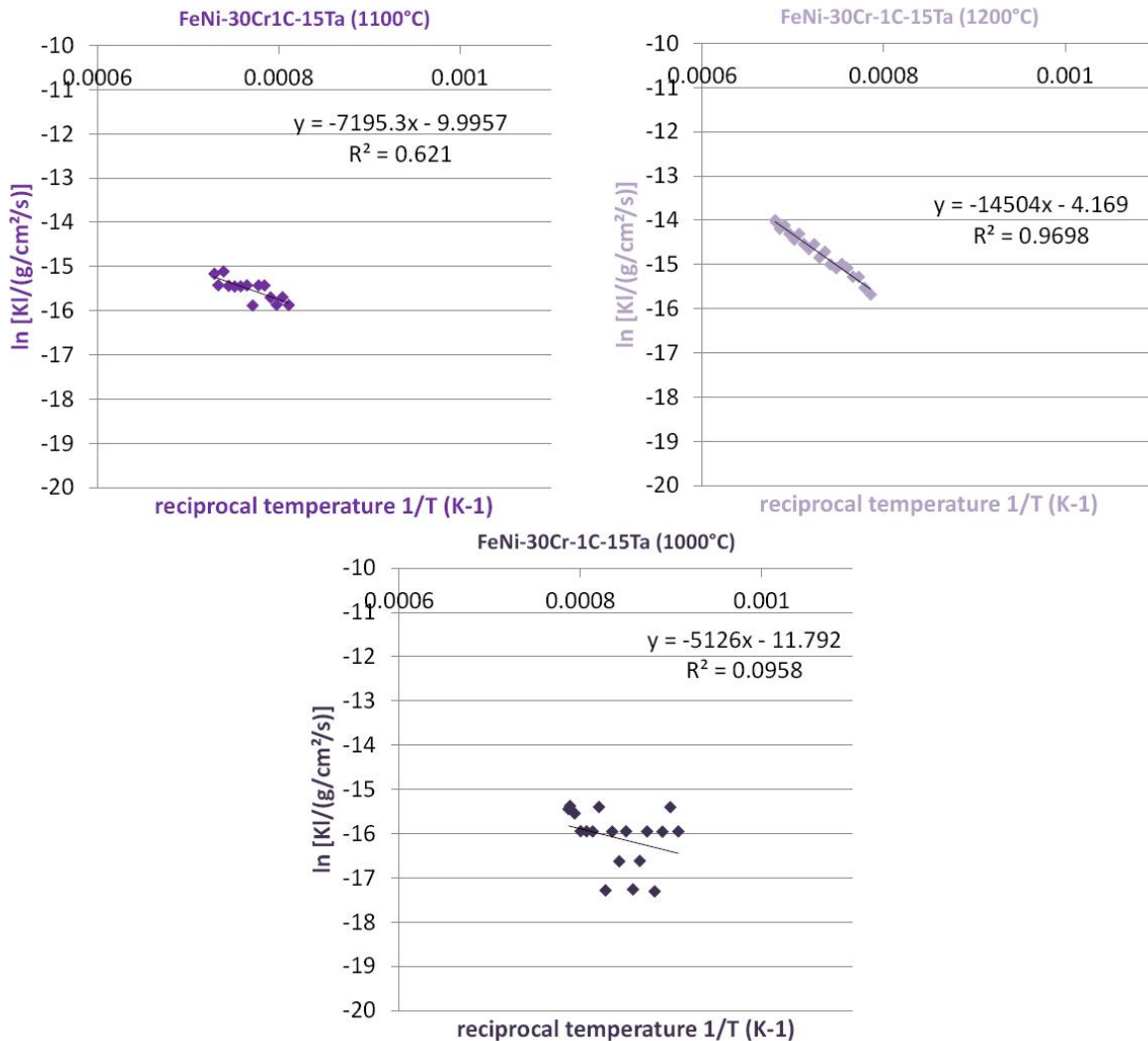


Figure 3 : Arrhenius plot of the instantaneous linear oxidation constant over the whole heating (or only a part if the point's cloud is not straight elongated); values of the slope of the regression straight line for deducing the values of activation energies (displayed in TABLE 2)

TABLE 2 : Values of the activation energies characterizing the dependence on temperature of the linear oxidation constant K_I issued from the successive values of K_I noted during the heating (over the linear part of the Arrhenius plot); value of the K_I value at the start of the isothermal stage

Q (J/Mol) issued from the $\ln ((d\Delta m/S)/dt)$ plot versus $1/T$ (K) during heating	1000°C-test	1100°C-test	1200°C-test
	42618	59822	120586
Final value of K_I (end of cooling, beginning of the isothermal stage ($\times 10^{-8}$ g/cm ² /s))	14.62	31.85	76.06
Mass gain at the end of heating (mg/cm ²)	0.078	0.114	0.356

whole heating are displayed in the third line of TABLE 2. The value is logically higher for a higher temperature.

Isothermal oxidation

When plotted as mass gain versus time the isothermal oxidation curves are not all parabolic. The one obtained for an isothermal stage temperature of 1000°C

is effectively really parabolic, with neither detectable jumps nor tendency to para-linear kinetic. In contrast the mass gain curves obtained for 1100°C and for 1200°C are very irregular since affected by mass gain jumps.

When plotted versus temperature (after having corrected the mass gain files from the air buoyancy varia-

Full Paper

TABLE 3 : Values of the temperatures at which the mass gain by oxidation during heating has become significantly high enough to be detected by the thermo-balance

Oxidation test	Mass gain at the end of heating (mg/cm ²); Proportion / heat.+isoth. (%)	Mass gain at the end of the isoth. stage (mg/cm ²) (sum of ← and →)	Isothermal mass gain (mg/cm ²); Proportion / heat.+isoth. (%)
1200°C-test	0.356 (4.80%)	7.420	7.064 (95.20%)
1100°C-test	0.114 (2.92%)	3.905	3.791 (97.08%)
1000°C-test	0.078 (5.58%)	1.399	1.321 (94.42%)

TABLE 4 : Values of the temperatures at which spallation started during the cooling and final mass variation after return at room temperature

Oxidation test	Temperature of start of the cooling-induced scale spallation (°C)	Final mass variation at the end of the whole thermal cycle (mg/cm ²)
1200°C-test	907.7	-2.44
1100°C-test	787.9	-2.57
1000°C-test	640.7	-1.48

tions) the three curves present a first part which quit the abscissa axis leading to the final mass gain already given in the last line of TABLE 2. Thereafter, in this type of representation the oxidation curve becomes a vertical straight line the length of which represents the part of mass gain which is isothermally realized. The values of this isothermal mass gain are given in TABLE 3 (last column). To obtain them the value of the mass gain at the end of the isothermal stage was read in the file and subtracted by the value of the total mass gain achieved during the heating (already given in TABLE 2 but reminded in TABLE 3). Logically the higher the temperature the higher the mass gain achieved during the 40 hours of isothermal oxidation. The calculation of the proportions in TABLE 3 shows that this isothermal mass gain is of course the major part of the total mass gain (94-97%) but it is also true that the mass gain already realized when the isothermal stage starts is significant (3-6% of the final mass gain before cooling).

Phenomena at cooling

The third part corresponds to the cooling during which oxidation may continue but slower and slower. After an eventual jump in mass gain, the mass decreases rapidly and irregularly: this is the spallation of the external oxide scale which starts at a given temperature and which leads to final mass which may be lower than the previous one if spallation was particularly severe. Some-

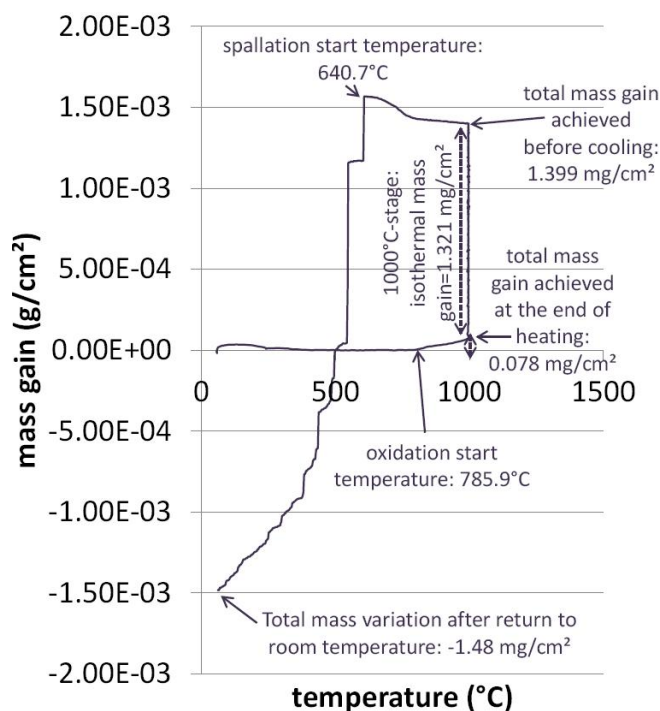


Figure 4 : The {mass gain versus temperature}-plot for the whole thermal cycle of the 1000°C-oxidation test

times final mass variations may be negative although that the main part of the experiment was characterized by a mass gain all the time before spallation start: the mass of oxygen remaining over the oxidized sample combined with the metallic elements may be lower than the mass of metallic elements lost as oxides when the scale – partly or wholly - quitted the samples. The val-

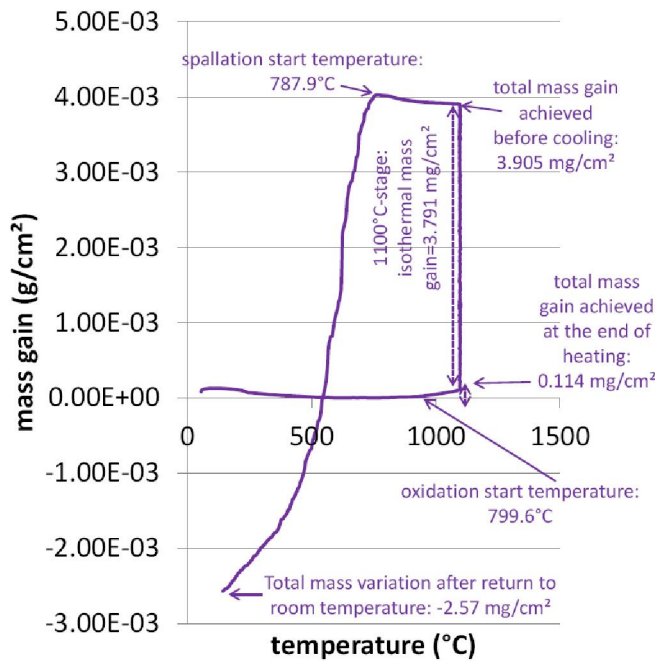


Figure 5 : The {mass gain versus temperature}-plot for the whole thermal cycle of the 1100°C-oxidation test

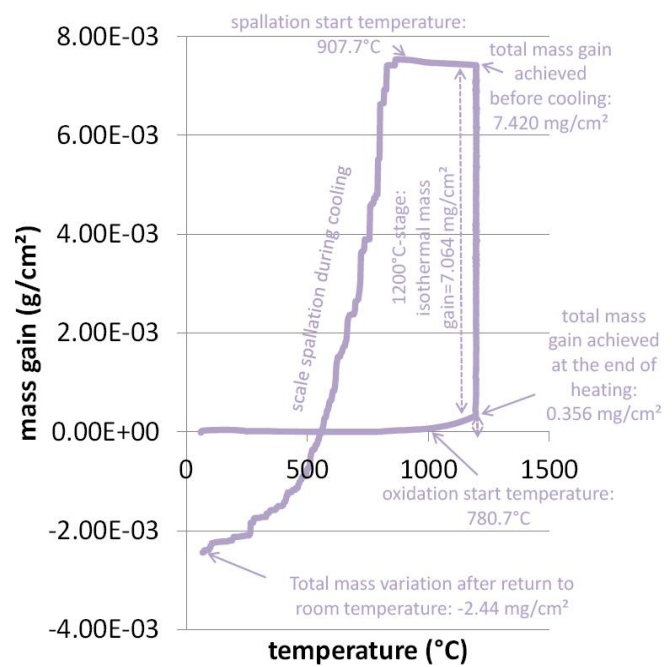


Figure 6 : The {mass gain versus temperature}-plot for the whole thermal cycle of the 1200°C-oxidation test

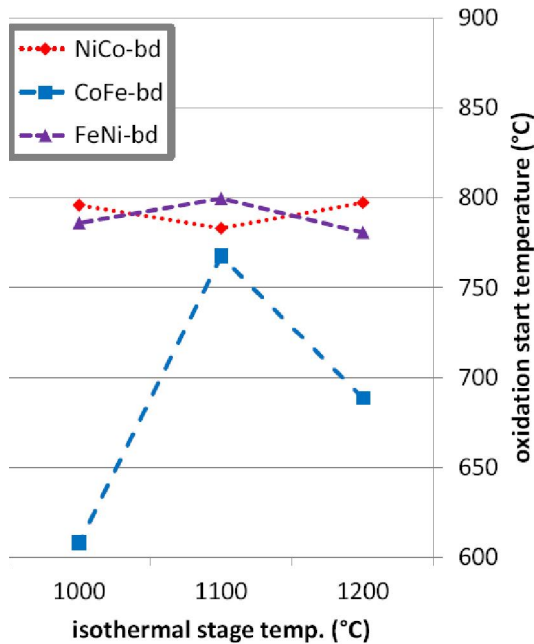
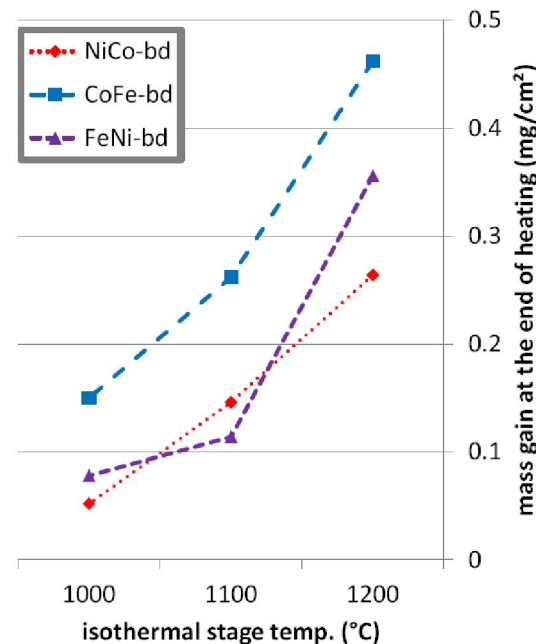


Figure 7 : Oxidation during the heating / comparison of the three alloys



ues of the temperatures at which oxide spallation started during the cooling for the three experiments as well as the final mass variations are given in TABLE 4. It appears that the spallation start temperature increases with the stage temperature.

Graphical summary

The whole curves plotted as mass gain versus temperature are presented in Figure 4 for the 1000°C-case,

Figure 5 for the 1100°C-case and in Figure 6 for the 1200°-case, with in each case the designation by arrows of the locations where the values of temperatures or of mass variations were red, as well as the obtained values already presented in the successive tables.

General commentaries

Globally the results obtained here do not seem being very different from the corresponding ones previ-

Full Paper

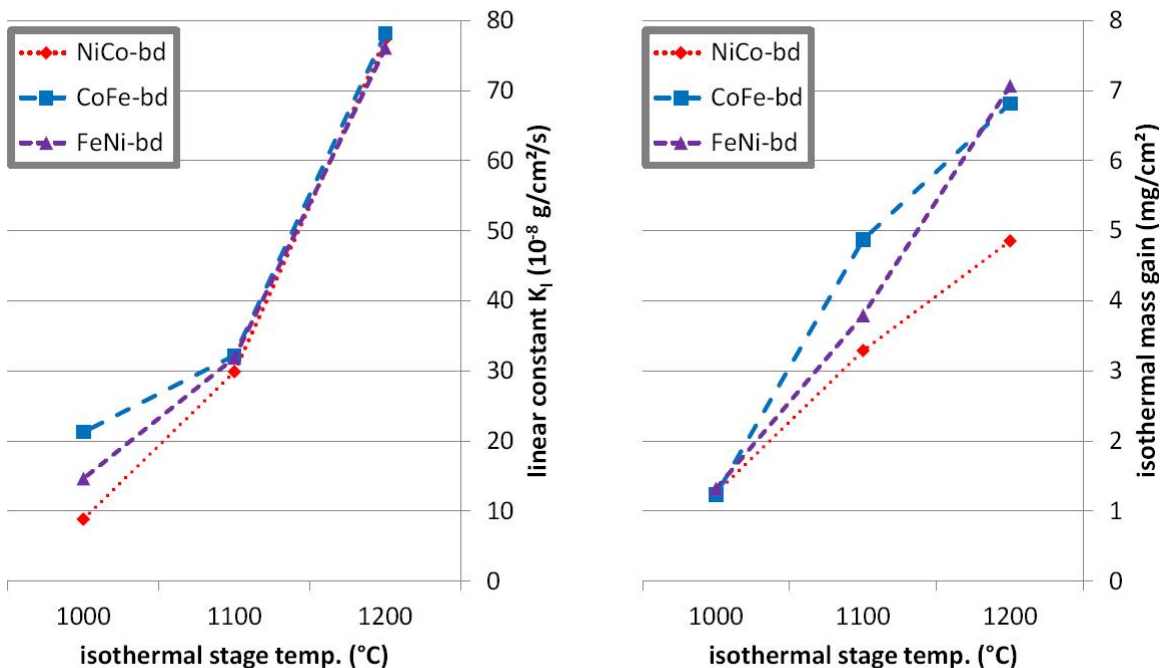


Figure 8 : Oxidation during the isothermal stage / comparison of the three alloys

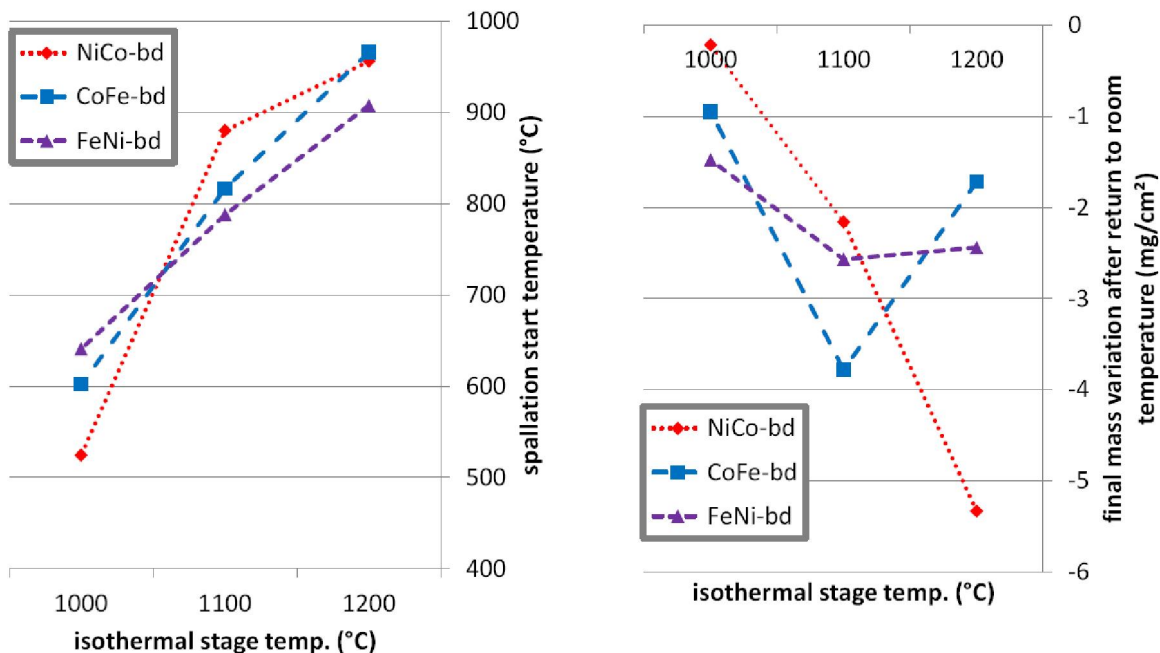


Figure 9 : Oxide spallation during the cooling / comparison of the three alloys

ously obtained for the CoFe-based alloy^[11] and for the NiCo-based one^[10]. To compare them more accurately additional graphics were elaborated.

Concerning the heating phase the variations of the oxidation start temperature (left) and of the total mass gain achieved during the heating (right) with the stage temperature are plotted in Figure 7. It clearly appears that oxidation starts sooner for the CoFe-based alloy

than for the two other ones, with as result a higher mass gain when temperature reaches the isothermal stage one.

Concerning the isothermal oxidation the variations of the linear oxidation constant at the beginning of the stage (left) and of the total mass gain achieved during the isothermal stage (right) with the stage temperature are plotted in Figure 8. It seems that the NiCo-based alloys oxidized slower than the two other alloys, as re-

vealed by the its generally lower values of initial linear constant and of whole isothermal mass gain.

Concerning the spallation of the oxide scales formed previously, the variations of the spallation start temperature (left) and of the final mass variation resulting from the whole thermal cycle (right) with the stage temperature are plotted in Figure 9. The results are more scattered and it is difficult to establish any order among the three alloys.

CONCLUSIONS

This third 30wt.%Cr-containing TaC-strengthened alloy based on two elements among nickel, cobalt and iron – the FeNi-based one – displayed globally the same type of microstructure as the two first alloys, and a behaviour in oxidation at high temperature which is not far from the ones of these first alloys. The overall oxidation rates are thus close to one another, all at a rather low level which is a good thing (despite the tendency of these alloys to scale detachment during the isothermal oxidation). The major problem is more the systematic loss - by the three alloys - of the oxide scales during the cooling although that this one is rather slow. This problem may become dramatic in case of frequent thermal cycling. To finish, as for the two alloys previously studied, these kinetic results obtained for this FeNi-based alloy will be soon enriched by metallographic ones^[12] to further interpretation and understanding.

REFERENCES

- [1] K.Kshitake, H.Era, F.Otsubo; *Scr.Metall.Mater.*, **24**, 1269 (1990).
- [2] A.Litwinchick, F.X.Kayser, H.H.Baker, A.Henkin; *J.Mater.Sci.*, **11**, 1200 (1976).
- [3] H.E.N.Stone; *J.Mater.Sci.*, **14**, 2787 (1979).
- [4] B.V.Cockeram; *Metall.Trans.A*, **33**, 3403 (2002).
- [5] A.Klimpel, L.A.Dobrzanski, A.Lisiecki, D.Janicki; *Journal of Materials Processing Technology*, **164-165**, 1068 (2005).
- [6] Z.T.Wang, H.H.Chen; *Mocaxue Xuebao Tribology*, **25**, 203 (2005).
- [7] H.Han, S.Baba, H.Kitagawa, S. A.Suilik, K.Hasezaki, T.Kato, K.Arakawa, Y.Noda; *Vacuum*, **78**, 27 (2005).
- [8] D.Zhang, X.Zhang; *Surface and Coating Technology*, **190**, 212 (2005).
- [9] K.Duretz, G.Pierson, P.Berthod; *Materials Science: An Indian Journal*, in press.
- [10] G.Pierson, K.Duretz, T.Schweitzer, E.Conrath, P.Berthod; *Materials Science: An Indian Journal*, submitted.
- [11] K.Duretz, G.Pierson, T.Schweitzer, E.Conrath, P.Berthod; *Materials Science: An Indian Journal*, submitted.
- [12] K.Duretz, G.Pierson, P.Villeger, P.Berthod, E.Conrath; *Materials Science: An Indian Journal*, to be submitted.